Interference and Outage in Mobile Random Networks: Expectation, Distribution, and Correlation

Zhenhua Gong, *Student Member, IEEE* and Martin Haenggi, *Senior Member, IEEE*

Abstract—In mobile networks, distance variations caused by node mobility generate fluctuations in the channel gains. Such fluctuations can be treated as another type of fading besides multi-path effects. In this paper, the interference statistics in mobile random networks are characterized by incorporating the distance variations of mobile nodes to the channel gain fluctuations. The mean interference is calculated at the origin and at the border of a finite mobile network. The network performance is evaluated in terms of the outage probability. Compared to a static network, the interference in a single snapshot does not change under uniform mobility models. However, random waypoint mobility increases (decreases) the interference at the origin (at the border). Furthermore, due to the correlation of the node locations, the interference and outage are temporally and spatially correlated. We quantify the temporal correlation of the interference and outage in mobile Poisson networks in terms of the correlation coefficient and conditional outage probability, respectively. The results show that it is essential that routing, MAC, and retransmission schemes need to be smart (*i.e,*. correlation-aware) to avoid bursts of transmission failures.

Index Terms—Correlation, interference, mobility, Poisson point process.

1 Introduction

1.1 Motivation

In wireless networks, interference is one of the central elements in system design, since network performance is often limited by competition of users for common resources [1]. There are four major sources of randomness that affect the interference in large networks. The first is multi-path fading, which is the time variation of the channel strengths due to small-scale effects. The second one is node placement. In mobile networks, a random model of spatial locations is necessary to facilitate the network analysis. A well-accepted model for the node distribution in wireless networks is the homogeneous Poisson point process (PPP) [2], [3], where the number of nodes in a certain region of area A is Poisson distributed with parameter $\lambda_0 A$, where λ_0 is the intensity. The numbers of nodes in disjoint regions are mutually independent. The third one is power control, which helps in the interference management, energy optimization, and connectivity [4]–[6]. When power control is implemented locally, the receiver is not aware of the power levels of other, interfering, transmitters, the power levels hence become a source of randomness in wireless networks. In this paper, however, we do not consider power control. The fourth one is channel access. ALOHA [7] and CSMA [8] are two classes of well-accepted random and distributed medium access control (MAC) protocols.

• *The authors are with the Wireless Institute, Department of Electrical Engineering, University of Notre Dame, Notre Dame, IN 46556, USA.*

For the sake of mathematical tractability and simplicity, the above four sources of randomness are often assumed identically and independently distributed (i.i.d.). For example, the channels are often assumed to be memoryless; if mobility is at all considered, the nodes are highly mobile so that the realizations of node locations are independent in different time slots; the node activities are not affected by previous activities. Are those assumptions realistic? In wireless networks, the i.i.d. assumptions for multi-path channel realizations, transmit power levels, and data traffic statistics are reasonable, if nodes transmit in short bursts. Furthermore, some broadband transmission techniques, such as frequency-hopping spread-spectrum, nullify the channel memories as well. For node placement, however, the situation is different. The correlation between node locations in different time slots is zero only if a completely new realization of the node placement is drawn in each time slot. Network models assuming independent realizations are impractical since the node velocities cannot be infinite. If the node placement follows a certain type of distribution such as a PPP in each time slot and the nodes do not have infinite mobility, the node locations in different time slots are correlated. An extreme case is a static but random network, where the nodes' positions are completely correlated, since the nodes do not move after their initial placement.

How does mobility affect network structure and performance? First, it is well known that multi-path fading is induced by *microscopic* mobility. A slight position change of a node induces randomness in channel gain. On the other hand, when distance is

considered in a wireless transmission, a significant change in the transmission distance, *macroscopic* mobility, gives rise to another degree of uncertainty: path-loss uncertainty. In this paper, we denote the multi-path fading simply as *fading* and large-scale path-loss uncertainty as *large-scale fading*. Both types of fading are induced by mobility. Second, mobility affects temporal and spatial correlation. The locations of a node always show a certain degree of correlation in different time slots, since the node speed is finite. The quantification of such correlation is important, since it greatly impacts the network performance.

1.2 Related work

There is a growing body of literature of large wireless networks with randomly distributed nodes. Stochastic geometry [9] and the theory of random geometric graphs [10] are two increasingly widely used analysis tools, which have been summarized in [2]. Interference and outage statistics are obtained in the case where nodes are Poisson distributed without multi-path fading [11], [12] and in the presence of fading [13], [14]. For the node placement models other than homogeneous Poisson, distance statistics in finite uniformly random networks are obtained in [15]. Interference and outage in clustered ad hoc networks are discussed in [16]. Interference results for ad hoc networks with general motion-invariant node distribution are presented in [17]–[19]. The interference distribution in doubly Poisson cognitive networks is analyzed in [20]. In [21], the hardcore point process is approximated by a non-homogeneous PPP to evaluate the outage. The performance of spatial relay networks is analyzed in [22], [23]. Routing in ad hoc networks is discussed in [13], [24]–[26]. The throughput and capacity in interference-limited networks have been derived in [27]–[29]. The spatio-temporal correlation of the interference and outage in static random networks has been studied in [30]. The spatial distribution of link outages in static random networks has been derived in [31]. The temporal correlation properties of the interference in static networks has been discussed in [32] in terms of the node locations, Rayleigh block fading, and traffic. In [33], the interference correlation is shown to induce diversity loss in Poisson neworks with multi-antenna receivers.

Related work on mobile networks includes [34], where a network of mobile nodes is mapped to a network of stationary nodes with dynamic links. In [35], different mobility models and their effects to ad hoc networks are compared. The stochastic properties of random walk and random waypoint mobility models are analyzed in [36] and [37]–[40], respectively. Another way of combining micro- and macroscopic path loss uncertainty has been explored in [41], where small-scale fading is interpreted as a distortion of the point process in modeling the node locations.

1.3 Our contributions

The main contributions of this paper are:

1) We calculate the mean interference at the origin and at the border of a finite network under different mobility models such as constrained i.i.d. mobility (CIM), random walk (RW), Brownian motion (BM), and random waypoint (RWP).
2) We characterize the interference and outage statistics in mobile random networks and investigate the effects of different mobility models to the network performance.
3) We quantify the temporal correlation of the interference and outage in mobile random networks, with concrete results on the correlation coefficient of the interference and conditional outage probability.
4) We suggest the design of transmission protocols with correlation-awareness.

1.4 Paper organization

The rest of the paper is organized as follows. System and mobility models are introduced in Section 2. In Section 3, the mean interference at the origin and at the border of a finite mobile network is calculated. The single-snapshot analysis of the interference and outage in mobile random networks is discussed in Section 4. In Section 5, the temporal correlation of the interference and outage is analyzed. Remarks and conclusions are presented in Section 6.

2 System model

2.1 Network model

We consider the link between a transmitter-receiver pair in a wireless network with the receiver at the origin o. Without loss of generality, the link distance is normalized to one (equivalently, we can say that the path-loss component is compensated for in the desired link). Other potential interferers are randomly distributed[1]. The initial node placement follows a Poisson point process $\Phi(0)$ on a domain $\mathbb{D} \subseteq \mathbb{R}^2$ with intensity λ_0. In a finite network as shown in Fig. 1 (left), $\mathbb{D} = B(o, R)$, where $B(o, R)$ is a disk of radius R centered at o. The number of nodes M inside $B(o, R)$ is Poisson distributed with mean $\lambda_0 \pi R^2$. In an infinite network as shown in Fig. 1 (right), $\mathbb{D} = \mathbb{R}^2$.

The nodes move independently of each other by updating their positions at the beginning of each time slot. In a finite network, nodes bounce back when they reach the boundary so that M remains constant. In an infinite network, all nodes move freely. In both cases, the locations of potential interferers follow a homogeneous or non-homogeneous PPP $\Phi(t) = \{x_i(t)\}$ at any time $t \in \mathbb{N}$.

1. We do not consider the assigned receivers of interfering transmitters, since they do not affect the network geometry in our analysis.

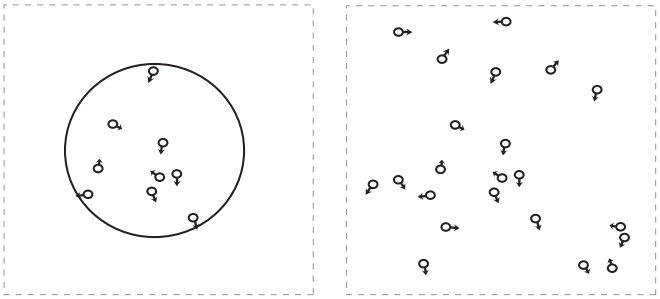

(a) Finite network (b) Infinite network

Fig. 1. Illustrations of finite and infinite mobile networks. The small circles denote mobile nodes and the arrows show the directions in which they will move in the next time slot. In (a), the nodes bounce back when they reach the boundary. In (b), all nodes move freely.

2.2 Mobility models

Different mobility models lead to different spatial properties of the networks and, in turn, affect the network performance differently [35]. In this part, we introduce several well-accepted models. For a fair comparison between different models, we first define the average speed of the nodes and set it to the same level. The speed of node i in one time slot is defined as $v_i(t) = \|x_i(t) - x_i(t-1)\|$, where $t \in \mathbb{N}$ and $\|\cdot\|$ is the Euclidean distance. We define

$$\bar{v} \triangleq \mathbb{E}[v_i(t)]. \tag{1}$$

$\bar{v}$ is the mean speed averaged over all nodes, or equivalently, over all times for a fixed node. The time slot is measured at the time scale of mobility, which is indicated Fig. 2(a). The mean distance that a node travels in one time slot is assumed much larger than the radio signal wavelength. The communication time scale, which will be introduced in the next sub-section, is much shorter or at the level of the mobility (see Fig. 2(b) and 2(c)).

2.2.1 Constrained i.i.d. mobility (CIM)

The CIM model is first introduced in [34]. Here, we consider an identical model except for the first time slot at $t = 0$. The node location $x_i(t)$ is

$$x_i(t) = x_i(0) + \bar{v} w_i(t), \tag{2}$$

where the home locations of the nodes are $\Phi(0) = \{x_i(0)\}$; $w_i(t)$ is uniformly at random in $B(x_i(0), \bar{v}R_{\text{CIM}})$. Using the results from [40], we calculate the normalized mobility range[2] $R_{\text{CIM}} = 45\pi/128 \approx 1.1045$. The CIM model is non-Markov. However conditioning on $x_i(0)$, we have $x_i(t)$ and $x_i(t+s)$ are i.i.d. for all $t, s > 0$.

2.2.2 Random walk (RW)

Under the RW model, a mobile node selects a new direction and speed randomly and independently in each time slot. Hence, the spatial node distribution remains uniform [36]. Mathematically, the location of node i at time $t+1$ for $t \in \mathbb{N}$ is

$$x_i(t+1) = x_i(t) + \bar{v} w_i(t), \tag{3}$$

where the distribution of $w_i(t)$ is uniformly at random in $B(x_i(t), \bar{v}R_{\text{RW}})$. The normalized mobility range $R_{\text{RW}} = 1.5$, which is straightforward.

2.2.3 Discrete-time Brownian motion (BM)

Under the discrete-time BM model, the node location at time $t+1$ for $t \in \mathbb{N}$ is

$$x_i(t+1) = x_i(t) + \bar{v} w_i(t), \tag{4}$$

where $w_i(t) = [w_{i,1}(t), w_{i,2}(t)]^T$ and $w_{i,1}(t)$ and $w_{i,2}(t)$ are i.i.d. normally distributed *i.e.*, $w_{i,1}(t), w_{i,2}(t) \sim \mathcal{N}(0, \sigma^2)$. After normalization, we have $\sigma = \sqrt{2/\pi}$.

Remark. From [13], [36, Lemma 2.2], and [42], the above mobility models with the bouncing behavior in a finite network[3] preserve the uniform properties of the node distribution. Consequently for any t, if the initial PPP is homogeneous, the PPP $\Phi(t)$ remains homogeneous. We categorize CIM, RW, and BM models as uniform mobility models (UMM).

2.2.4 Random waypoint (RWP)

This model is only strictly defined in a finite region. Each node uniformly chooses a destination in the region and moves towards it with randomly selected speed[4]. A new direction and speed are chosen only after the node reaches the destination. Otherwise, it keeps the same direction and speed for several time slots. The steady-state node distribution is a *non-uniform* distribution [38]. We denote the distance of a typical node to the origin at steady state by L. For $\mathbb{D} = B(o, R)$, the probability density function (pdf) of L is given by

$$f_L(r) = \frac{1}{R^2}\left(-\frac{4r^3}{R^2} + 4r\right). \tag{5}$$

The intensity measure of the point process follows as

$$\Lambda(B(o,r)) \triangleq \mathbb{E}(\Phi(B(o,r))) = 2\lambda_0 \pi r^2 - \frac{\lambda_0 \pi r^4}{R^2},$$

where $r \leqslant R$. The intensity function is thus given by

$$\lambda(x) \triangleq \lambda_\infty(x) = 2\lambda_0 - \frac{2\lambda_0 \|x\|^2}{R^2}. \tag{6}$$

2.3 Channel access scheme

We assume that transmissions start at the beginning of each time slot and that each transmission is finished within one time slot as shown in Fig. 2(b) and 2(c). The next transmission (if the node is scheduled to transmit)

2. The term "normalized" means that the average node speed is equal to one.

3. A more detailed discussion on the border behavior and effects in mobile networks is presented in [37].

4. In the simulations, the speed is chosen so that the travel distance is a multiple of the speed.

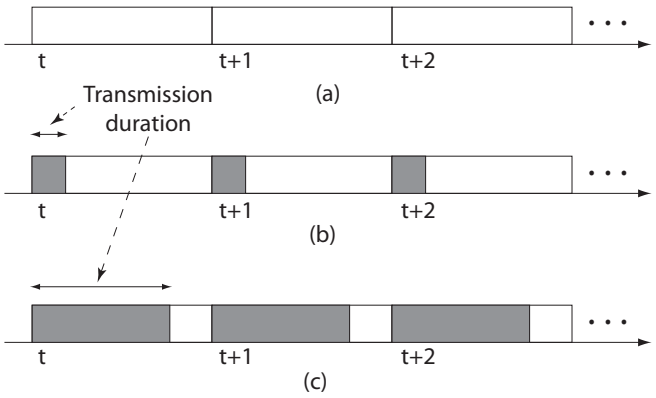

Fig. 2. Mobility and transmission time scales. The mobility (time) slots are indicated in (a). If a node is scheduled to transmit, each transmission period, which is presented in gray, is assumed to start at the beginning of each mobility slot. In (b), the transmission duration is much shorter than the mobility (time) slot; in (c), the length of transmission time is comparable to the mobility slot.

starts at the beginning of the next mobility (time) slot. Slotted ALOHA is assumed as the MAC protocol. In every time slot t, each node determines whether to transmit or not independently with probability p. This channel access scheme minimizes the correlation. Note that the model is also suitable for the case where not all transmissions start at the beginning of a mobility time slot, since spreading out the transmissions using time division scheduling reduces the density of interferers. This case is modeled by reducing the transmit probability p by an appropriate factor.

2.4 Channel model

The attenuation in the wireless channel is modeled as the product of a large-scale path-loss component and a small-scale fading component. The path-loss function $g(x)$ is given by

$$g(x) = \frac{1}{\epsilon + \|x\|^{\alpha}}, \qquad \epsilon \geqslant 0, \tag{7}$$

where α is the path loss exponent. Two categories of models are usually considered: the singular path-loss model where $\epsilon = 0$ and the non-singular path-loss model where $\epsilon > 0$. $rg(r) = r/(\epsilon + r^{\alpha})$ is assumed to be integrable, *i.e.*,

$$\int_{\nu}^{\infty} rg(r)\mathrm{d}r < \infty, \qquad \forall \nu > 0.$$

$\alpha > 2$ is necessary and sufficient to satisfy the integrability condition.

For the multi-path fading, we consider a deterministic model (*i.e.,* no fading) and the Rayleigh and Nakagami fading models in the desired link and the interfering links. In Rayleigh fading, the pdf of the power fading gain h is given by

$$f_h(x) = \exp(-x).$$

In the more general Nakagami-m fading model, the pdf of the power fading gain is given by

$$f_h(x) = \frac{m^m x^{m-1} \exp(-mx)}{\Gamma(m)}, \qquad m > 0.$$

If the transmission duration is relatively long, *i.e.*, comparable to the length of the mobility (time) slot (Fig. 2(c)), the packet may observe a large number of realizations, since the node covers many wavelengths in distance. With interleaving, the fading will then have a negligible effect corresponding to a large m or even $m \to \infty$ (no fading). If the transmissions are short (Fig. 2(b)), on the other hand, fading needs to be accounted for using the Rayleigh or Nakagami models with small m.

2.5 Total interference and outage probability

At time t, the total interference at the receiver (located at z) is given by

$$I(t) = \sum_{x \in \Phi(t)} T_x(t) h_x(t) g(x - z), \tag{8}$$

where the random variables $T_x(t)$ are i.i.d. Bernoulli with parameter p due to ALOHA; $h_x(t)$ is the multi-path fading with mean $\mathbb{E}h = 1$.

The outage probability p_{o} is one of the fundamental performance metrics in wireless networks. In interference-limited channels, an outage occurs if the signal-to-interference ratio (SIR) at a receiver is lower than a certain threshold θ *i.e.*,

$$p_{\mathrm{o}} \triangleq \mathbb{P}(\mathrm{SIR} < \theta). \tag{9}$$

3 Mean Interference

In this section, we calculate the mean interference in a network under either UMM or RWP mobility. For $\epsilon > 0$ and $\alpha = 4$, it is known [5] that the mean interference at the origin under UMM is given by

$$\mathbb{E}[I_{o,\mathrm{UMM}}] = \frac{\pi p \lambda_0}{\sqrt{\epsilon}} \arctan \frac{R^2}{\sqrt{\epsilon}}. \tag{10}$$

We have the following proposition about the mean interference at the origin under the RWP model.

Proposition 1. *For $\alpha = 4$, a finite network of radius R, and ALOHA with parameter p, The mean interference at the origin under the RWP model is given by*

$$\mathbb{E}[I_{o,\mathrm{RWP}}] = \frac{2\pi p \lambda_0}{\sqrt{\epsilon}} \arctan \frac{R^2}{\sqrt{\epsilon}} - \frac{p\lambda_0 \pi}{R^2} \ln\left(1 + \frac{R^4}{\epsilon}\right). \tag{11}$$

As $R \to \infty$,

$$\mathbb{E}[I_{o,\mathrm{RWP}}] \lesssim 2\mathbb{E}[I_{o,\mathrm{UMM}}], \tag{12}$$

where "$\lesssim$" denotes an upper bound with asymptotic equality.

Proof: Under the RWP model, we have from Campbell's theorem

$$\mathbb{E}[I_{o,\mathrm{RWP}}] = 4\pi p\lambda_0 \int_0^R \left(\frac{r}{\epsilon + r^4} - \frac{r^3}{\epsilon + r^4}\right) \mathrm{d}r.$$

The rest of the calculation is straightforward. □

For $\epsilon = 0$, we ignore the interfering nodes which are very close to the origin by setting a guard zone[5] $B(0, \nu)$, for any $\nu > 0$. We have the following proposition about the mean interference at the origin.

Proposition 2. *For a finite network of radius R and ALOHA parameter p, the mean interference at the origin under UMM is given by*

$$\mathbb{E}[I_{o,\mathrm{UMM}}] = \frac{2p\lambda_0\pi}{\alpha - 2}\left(\nu^{-\alpha+2} - R^{-\alpha+2}\right), \qquad (13)$$

where ν is the guard radius in the singular path-loss model. For $\alpha = 4$, the mean interference at the origin under the RWP model is given by

$$\mathbb{E}[I_{o,\mathrm{RWP}}] = 2p\lambda_0\pi\left(\nu^{-2} - R^{-2}\right) - \frac{4p\lambda_0\pi}{R^2}\ln\frac{R}{\nu}. \qquad (14)$$

For $\alpha \neq 4$, we have

$$\begin{aligned}\mathbb{E}[I_{o,\mathrm{RWP}}] &= \frac{4p\lambda_0\pi}{\alpha - 2}\left(\frac{1}{\nu^{\alpha-2}} - \frac{1}{R^{\alpha-2}}\right) \\ &\quad - \frac{4p\lambda_0\pi}{(\alpha-4)}\left(\frac{1}{\nu^{\alpha-4}R^2} - \frac{1}{R^{\alpha-2}}\right). \qquad (15)\end{aligned}$$

As $R \to \infty$, we obtain again,

$$\mathbb{E}[I_{o,\mathrm{RWP}}] \lesssim 2\mathbb{E}[I_{o,\mathrm{UMM}}].$$

Proof: Under UMM,

$$\mathbb{E}[I_{o,\mathrm{UMM}}] = 2\pi p\lambda_0 \int_\nu^R r^{-\alpha+1}\mathrm{d}r.$$

and under the RWP model,

$$\mathbb{E}[I_{o,\mathrm{RWP}}] = 4\pi p\lambda_0 \int_\nu^R r^{-\alpha+1} - \frac{r^{-\alpha+3}}{R^2}\mathrm{d}r.$$

□

From Proposition 1 and 2, we find that the mean interference at the origin under the RWP model is asymptotically twice the mean interference under UMM when the radius R grows large.

Next we evaluate the mean interference at the border of a network (*i.e.*, at any z with $\|z\| = R$). For UMM, we have the following proposition.

Proposition 3. *For $\alpha = 4$, a finite network of radius R, and ALOHA parameter p, the mean interference at a border location z with $\|z\| = R$ under UMM is given by*

$$\mathbb{E}[I_{R,\mathrm{UMM}}] = \frac{p\lambda_0}{\sqrt{\epsilon}}\int_0^1 \frac{\arctan\frac{4R^2}{\sqrt{\epsilon}}x^2}{\sqrt{1-x^2}}\mathrm{d}x, \qquad \epsilon > 0. \qquad (16)$$

5. The guard zone is set to keep the mean interference finite.

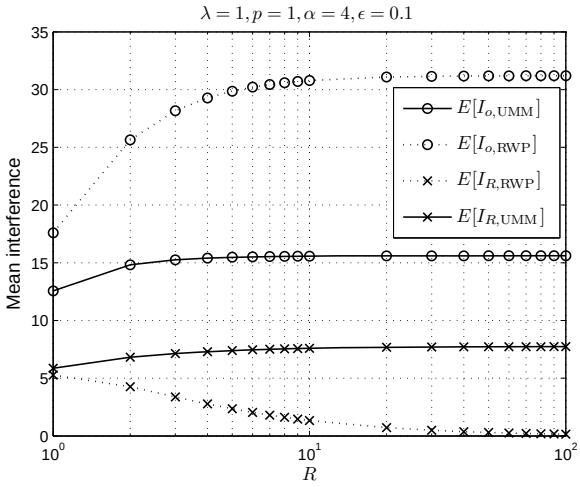

Fig. 3. The mean interference at the origin o and at the border location z, $\|z\| = R$, under the non-singular path-loss model.

When $R \to \infty$, we have

$$\lim_{R\to\infty}\mathbb{E}[I_{R,\mathrm{UMM}}] = \frac{p\lambda_0\pi^2}{4\sqrt{\epsilon}}, \qquad \epsilon > 0. \qquad (17)$$

Under the RWP model, we have

$$\lim_{R\to\infty}\mathbb{E}[I_{R,\mathrm{RWP}}] = 0. \qquad (18)$$

Proof: We have

$$\begin{aligned}\mathbb{E}[I_{R,\mathrm{UMM}}] &= p\lambda_0\int_{B((R,0),R)} g(x)\mathrm{d}x \\ &= p\lambda_0\int_{-\pi/2}^{\pi/2}\int_0^{2R\cos\theta} rg(r)\mathrm{d}r\mathrm{d}\theta,\end{aligned}$$

which equals (16). For the RWP model, the mean interference at the border is given by

$$\begin{aligned}\mathbb{E}[I_{R,\mathrm{RWP}}] &= p\int_{B(0,R)}\lambda(x)g(x-z)\mathrm{d}x \\ &= \frac{2p\lambda_0}{R^2}\int_{-\pi/2}^{\pi/2}\int_0^{2R\cos\theta}\frac{2Rr^2\cos\theta - r^3}{\epsilon + r^\alpha}\mathrm{d}r\mathrm{d}\theta.\end{aligned}$$

Letting $R \to \infty$, we obtain (18). □

The following corollary follows from (10) and (17).

Corollary 4. *Assume UMM, $\alpha = 4$, and a finite network of radius R. When $R \to \infty$,*

$$\mathbb{E}[I_{R,\mathrm{UMM}}] \lesssim \frac{1}{2}\mathbb{E}[I_{o,\mathrm{UMM}}]. \qquad (19)$$

Fig. 3 shows the mean interference at the origin o and at the border under the non-singular path-loss model. Both UMM and RWP model are considered. $\mathbb{E}[I_{R,\mathrm{RWP}}]$ decreases with R since the node intensity at the border decreases with increasing R.

4 Single-snapshot analysis of interference and outage

In this section, we evaluate the network performance in a single snapshot. We assume that $\epsilon = 0$. The mobility models in Section 2.2 are separated into two categories: uniform and non-uniform.

4.1 Interference in uniformly mobile networks

Because of the uniformity of the mobility, the mobile network in any time t can be treated as a correlated realization of a static network. Hence the existing results of the interference and outage in static networks in [5], [11] also apply to uniformly mobile networks.

4.2 Interference in non-uniformly mobile networks

4.2.1 Interference in finite networks without fading

We consider RWP and set $\mathbb{D} = B(o, R)$. We evaluate the interference at the origin o, since the interferer density decreases with the distance to the origin o (see (6)), which leads to a lower bound of the network performance. As we are only interested in the interference distribution in a single time slot, we can drop the dependence on t and focus on the generic random variable

$$I = \sum_{x \in \Phi} T_x \left\| x \right\|^{-\alpha}. \tag{20}$$

There is no closed-form expression for the pdf of the interference in most cases. However, since the received power decays according to a power law, only considering the interference from the nearest interferer to the receiver provides a good approximation, if the path-loss exponent α is not too close to 2 [5]. Therefore, the interference power is approximately

$$I \approx I_1 = R_1^{-\alpha}, \tag{21}$$

where R_1 is the distance between the origin to its nearest interferer. Given a total number of nodes M, we have

$$\begin{aligned} \mathbb{P}\left(R_1 \leqslant r \mid M\right) &= 1 - \left(1 - F_L(r)\right)^M \\ &= 1 - \left(1 - \left(\frac{2r^2}{R^2} - \frac{r^4}{R^4}\right)\right)^M, \end{aligned}$$

where $F_L(r) = \int_0^r f_L(x)\mathrm{d}x$ and $f_L(x)$ is given in (5). Since M is Poisson distributed with mean $p\lambda_0\pi R^2$, the pdf of R_1 is thus given by

$$\begin{aligned} f_{R_1}(r) &= \frac{\mathrm{d}\mathbb{E}_M\left[\mathbb{P}\left(R_1 \leqslant r \mid M\right)\right]}{\mathrm{d}r} \\ &= p\lambda_0\pi\left(4r - 4\frac{r^3}{R^2}\right) e^{-p\lambda_0\pi\left(2r^2 - \frac{r^4}{R^2}\right)}. \end{aligned} \tag{22}$$

From (21) and (22), we obtain the pdf of I_1:

$$f_{I_1}(x) = 2p\lambda_0\pi\delta\left(x^{-\delta-1} - \frac{x^{-2\delta-1}}{R^2}\right) e^{-p\lambda_0\pi\left(2x^{-\delta} - \frac{x^{-2\delta}}{R^2}\right)}, \tag{23}$$

where $\delta \triangleq 2/\alpha$. With deterministic channels, a simple lower bound on the outage probability is derived using the nearest-interferer approximation:

$$\begin{aligned} p_{\mathrm{o}}^{\mathrm{nf}}(\theta) \triangleq \mathbb{P}\left(\frac{1}{I} < \theta\right) &\geqslant \mathbb{P}\left(\frac{1}{I_1} < \theta\right) \\ &= 1 - F_{I_1}(\theta^{-1}) \triangleq \underline{p}^{\mathrm{nf}}(\theta). \end{aligned}$$

Calculating explicitly, we have

$$\underline{p}^{\mathrm{nf}}(\theta) = 1 - \exp\left(-p\lambda_0\pi\left(2\theta^{\delta} - \frac{\theta^{2\delta}}{R^2}\right)\right). \tag{24}$$

4.2.2 Interference in finite networks with fading

When channels are subject to multi-path fading, the interference power from the nearest interferer is $h_1 I_1$, where h_1 is the multi-path fading coefficient. Then the lower bound of the outage probability is given by

$$\underline{p}^{\mathrm{f}}(\theta) = \mathbb{E}_H\left[\mathbb{P}\left(I_1 > \frac{H}{\theta} \mid H\right)\right],$$

where $H \triangleq h/h_1$ and h is the fading gain in the desired link. In the Rayleigh fading case, the pdf of H is given by

$$f_H(x) = \frac{1}{(x+1)^2}.$$

We then obtain

$$\underline{p}^{\mathrm{f}}(\theta) = 1 - \int_0^{\infty} \frac{\exp\left(-p\lambda_0\pi\left(2\theta^{\delta}x^{-\delta} - \frac{\theta^{2\delta}x^{-2\delta}}{R^2}\right)\right)}{(x+1)^2}\mathrm{d}x. \tag{25}$$

The lower bounds of the outage probabilities and the simulation results are presented in Fig. 4. For comparison, the lower bounds and simulation results under the RW model are also included. The expected number of nodes in the region $\mathbb{E}[M] = 10\pi \approx 31$. From the figure, we find that the nearest-interferer approximation provides a close approximation in terms of the outage probability, in particular in the lower threshold regime (small θ), which is the regime of practical interest. Furthermore, multi-path fading is harmful to the link connections in mobile networks.

4.2.3 Interference in infinite networks

In infinite networks ($\mathbb{D} = \mathbb{R}^2$), the RWP model cannot be properly defined. However, we can derive the Laplace transform of the total interference if the node distance distribution follows (5). The Laplace transform of the interference is first calculated under a finite radius R, and then we let $R \to \infty$. Since the mobility model itself can not be defined, such a result is not the interference characterization under the RWP model in infinite networks, but it provides an asymptotic expression as R gets large.

Proposition 5. *For $R \to \infty$, the Laplace transform of the total interference converges to*

$$\mathcal{L}_I(s) = \exp\left(-2\pi\lambda_0 p s^{\delta}\mathbb{E}[h^{\delta}]\Gamma\left(1-\delta\right)\right). \tag{26}$$

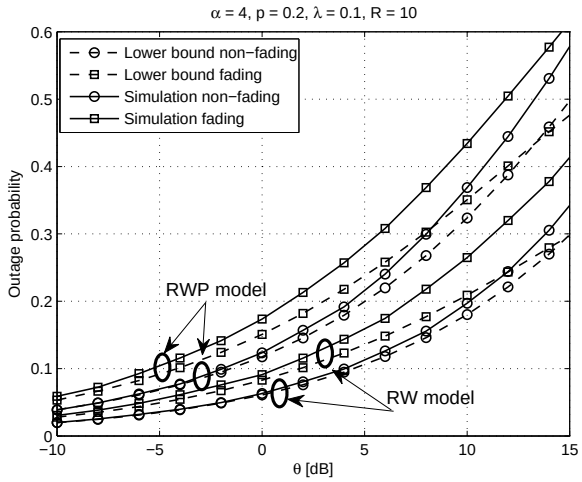

Fig. 4. Simulation results versus the corresponding lower bounds of the outage probability for different fading and mobility models.

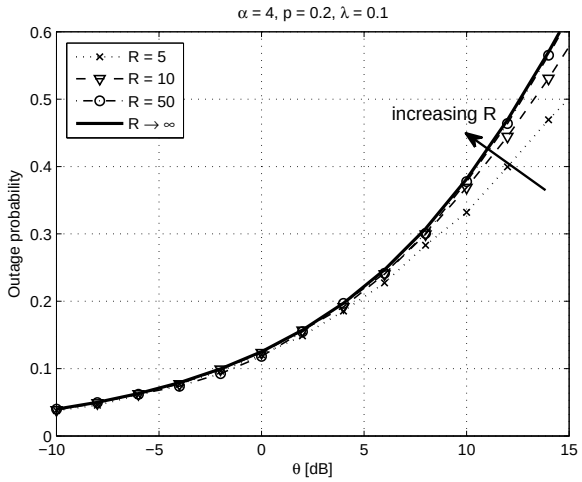

Fig. 5. The outage probabilities under the RWP mobility with different radii R for the case without fading. The bound (solid curve) is obtained from (28). The curves with finite R are simulation results.

Proof: We start with a finite network of radius R. From (6), the radial transmitter intensity function is given by

$$\lambda(r) = 4p\lambda_0\pi r - \frac{4p\lambda_0\pi r^3}{R^2}.$$

Using the probability generating functional (pgfl) to calculate the Laplace transform, we obtain

$$\mathcal{L}_I(s) = \exp\left(-\mathbb{E}_h\left[\underbrace{\int_0^R \left(1-\exp\left(-shr^{-\alpha}\right)\right)\lambda(r)\mathrm{d}r}_{A(h)}\right]\right). \quad (27)$$

For the integral $A(h)$, we have

$$A(h) = \int_0^R 4\pi p\lambda_0 r\left(1-e^{-shr^{-\alpha}}\right)\mathrm{d}r - \frac{p\lambda_0\pi}{R^{-2}}\left(1-e^{-shR^{-\alpha}}\right) - \int_0^R \frac{\alpha p\lambda_0\pi shr^{-\alpha+3}}{R^2}e^{-shr^{-\alpha}}\mathrm{d}r.$$

Letting $R\to\infty$ and using the L'Hopital's rule, we obtain

$$\lim_{R\to\infty}\frac{1-e^{-shR^{-\alpha}}}{R^{-2}} = \frac{\alpha shR^{-\alpha-1}e^{-shR^{-\alpha}}}{-2R^{-3}} \overset{(a)}{=} 0,$$

where (a) holds for $\alpha>2$, and

$$\lim_{R\to\infty}\int_0^R \frac{r^{-\alpha+3}}{R^2}e^{-shr^{-\alpha}}\mathrm{d}r = \lim_{R\to\infty}\frac{R^{-\alpha+2}e^{-shR^{-\alpha}}}{2} = 0.$$

Therefore, we have

$$\lim_{R\to\infty} A(h) = 2\lambda_0\pi s^\delta h^\delta\Gamma(1-\delta).$$

Inserting this into (27) yields the result. □

Comparing (26) with [11, (18)], we notice that at the center of a large disk, the interference generated by RWP nodes is asymptotically equivalent to the interference generated by nodes of uniformly mobility with *doubled* node intensity as the disk radius $R\to\infty$, which is in agreement with (12). Without fading, the outage probability ($\alpha=4$) is given by

$$p_{\mathrm{o}}^{\mathrm{nf}}(\theta) = \mathbb{P}(I>\theta^{-1}) = \mathrm{erf}\left(p\pi^{\frac{3}{2}}\sqrt{\theta}\lambda_0\right), \quad (28)$$

where $\mathrm{erf}(x) = 2\int_0^x e^{-t^2}\mathrm{d}t/\sqrt{\pi}$ is the error function.

Fig. 5 shows the outage probabilities for RWP nodes with different radii R by simulations versus the asymptotic bound. The bound, which is exact for $R\to\infty$, is calculated using (28). The simulation curves approach the bound quickly as R increases. Hence, (28) can be viewed as the upper bound and the asymptotic expression of the outage probability for large R. For Rayleigh fading, since $\mathbb{E}[h^\delta]=\Gamma(1+\delta)$,

$$p_{\mathrm{o}}^{\mathrm{f}}(\theta) = 1-\mathcal{L}_I(\theta) = 1-\exp\left(-\frac{2p\pi^2\lambda_0\delta\theta^\delta}{\sin(\pi\delta)}\right). \quad (29)$$

The same extra factor 2 is obtained as we compare (29) to the homogeneous case [28, (6)], which confirms that RWP mobility increases the interference and outage at the origin.

4.3 Tightness of the outage lower bound

In this part, we evaluate the tightness of the outage lower bound we have obtained in finite networks. For deterministic or Rayleigh fading channel, we have the following proposition.

Proposition 6. *When $\theta\to 0$, the outage probability $p_{\mathrm{o}}(\theta)$ and the outage lower bound $\underline{p}(\theta)$ have the following relationship*

$$\underline{p}(\theta) \sim p_{\mathrm{o}}(\theta). \quad (30)$$

Proof: First we consider the case without multi-path fading. With similar steps in [11], the ccdf of the

interference in the infinite case is given by

$$F_I(x) = \frac{1}{\pi}\sum_{k=1}^{\infty}\frac{\Gamma(\alpha k)}{k!}\left(\frac{2\lambda_0 p\pi\Gamma(1-\delta)}{x^{\delta}}\right)^k \sin(k\pi(1-\alpha)). \tag{31}$$

The term $2\lambda_0$ in (31) instead of λ_0 in [11, (23)] is the difference between the RWP and uniform mobility cases. We then have

$$\begin{aligned}\lim_{\theta\to 0}\frac{p^{\mathrm{nf}}(\theta)}{p_{\mathrm{o}}^{\mathrm{nf}}(\theta)} &= \lim_{\theta\to 0}\frac{1-\exp\left(-p\lambda_0\pi\left(2\theta^{\delta}-\frac{\theta^{2\delta}}{R^2}\right)\right)}{\frac{1}{\pi}\sum_{k=1}^{\infty}\frac{\Gamma(\alpha k)}{k!}(2\lambda_0 p\pi\Gamma(1-\delta)\theta^{\delta})^k}\\ &\overset{(a)}{=} \lim_{\theta\to 0}\frac{p\lambda_0\pi^2\left(2\delta\theta^{\delta-1}-\frac{2\delta\theta^{2\delta-1}}{R^2}\right)e^{-p\lambda_0\pi\left(2\theta^{\delta}-\frac{\theta^{2\delta}}{R^2}\right)}}{\sum_{k=1}^{\infty}\frac{\Gamma(\alpha k)}{k!}\delta k\theta^{\delta k-1}\left(2\lambda_0 p\pi\Gamma(1-\delta)\right)^k}\\ &\overset{(b)}{=} 1,\end{aligned}$$

where (a) holds because of the L'Hopital's rule; (b) holds because of the dominance of the term for $k=1$ in the Taylor series expansion.

Second, we consider Rayleigh fading. From (25) and (29), we have

$$\begin{aligned}&\lim_{\theta\to 0}\frac{p^{\mathrm{f}}(\theta)}{p_{\mathrm{o}}^{\mathrm{f}}(\theta)}\\ &\overset{(a)}{=} \lim_{\theta\to 0}\frac{\int_0^{\infty}\frac{x^{-\delta}}{(x+1)^2}\exp\left(-p\lambda_0\pi\left(2\theta^{\delta}x^{-\delta}-\frac{\theta^{2\delta}x^{-2\delta}}{R^2}\right)\right)\mathrm{d}y}{\frac{\pi\delta}{\sin(\pi\delta)}\exp\left(-\frac{2p\pi^2\lambda_0\delta\theta^{\delta}}{\sin(\pi\delta)}\right)}\\ &= 1,\end{aligned} \tag{32}$$

where (a) holds because of L'Hopital's rule. □

5 Temporal Correlation of Interference and Outage

The interference statistics in mobile networks in a single time slot have been studied in the previous section, with concrete results also for the outage statistics. However, only investigating the interference in a single time slot is insufficient to design the transmission and routing schemes in wireless networks, since the interference is temporally and spatially correlated. Such correlation, which is caused by the locations of mobile nodes, affects retransmission and routing strategies greatly. For example in an ARQ (Automatic Repeat reQuest) retransmission mechanism, a packet is retransmitted after a timeout or after a negative acknowledgment (NACK) received. Intuitively when a link is in outage and correlation is high, blind retransmissions lead to a higher failure rate than for independent interference. Quantifying the correlation is hence necessary. In this section, we consider uniform mobility models only and focus on infinite networks ($\mathbb{D}=\mathbb{R}^2$). We assume that $\epsilon > 0$ in the path-loss expression in (7), since for $\epsilon = 0$ some integrals (such as the mean interference) are infinite.

5.1 Temporal correlation of interference

In this part, we analyze the temporal correlation of the interference. The spatio-temporal correlation can be treated similarly. Because of the spatial stationarity of the point process, it is sufficient to consider the interference at the origin. The total interference in (8), $I(t)$, is identically distributed for any $t \in \mathbb{N}$. We denote the temporal correlation coefficient of the interference between time s and t as $\rho_\tau \triangleq \rho_{I(t)I(s)}$, where $\tau = |t-s|$. We have the following proposition about ρ_τ.

Proposition 7. *The temporal correlation coefficient of the interferences $I(s)$ and $I(t)$, where $s \neq t$, is given by*

$$\rho_\tau = \frac{p\int_{\mathbb{R}^2} g(x)\mathbb{E}_{w_\tau}[g(x+\bar{v}w_\tau)]\mathrm{d}x}{\mathbb{E}[h^2]\int_{\mathbb{R}^2} g^2(x)\mathrm{d}x} \leqslant \frac{p}{\mathbb{E}[h^2]}, \tag{33}$$

where $\bar{v}w_\tau$ is the location difference of a node between time s and t.

Proof: Since $I(s)$ and $I(t)$ are identically distributed, we have

$$\rho_\tau \triangleq \frac{\mathrm{Cov}(I(t),I(s))}{\mathrm{Var}[I(t)]} = \frac{\mathbb{E}[I(t)I(s)]-\mathbb{E}[I(t)]^2}{\mathbb{E}[I(t)^2]-\mathbb{E}[I(t)]^2}. \tag{34}$$

The mean product of $I(t)$ and $I(s)$ ($t \neq s$) is given by

$$\begin{aligned}&\mathbb{E}[I(t)I(s)]\\ &= \mathbb{E}\left[\sum_{x\in\Phi(t)}T_x(t)h_x(t)g(x)\sum_{y\in\Phi(s)}T_y(s)h_y(s)g(y)\right]\\ &= \mathbb{E}\left[\sum_{x\in\Phi(s)}T_x(t)h_x(t)g(x+\bar{v}w_\tau)\sum_{y\in\Phi(s)}T_y(s)h_y(s)g(y)\right]\\ &= \mathbb{E}\left[\sum_{x\in\Phi(s)}T_x(t)T_x(s)h_x(t)h_x(s)g(x+\bar{v}w_\tau)g(x)\right]+\\ &\quad \mathbb{E}\left[\sum_{x,y\in\Phi(s)}^{x\neq y}T_x(t)T_y(s)h_x(t)h_y(s)g(x+\bar{v}w_\tau)g(y)\right],\end{aligned} \tag{35}$$

where $\bar{v}w_\tau$ is the location difference of a node between time s and t. Conditioning on w_τ and following the proof of Lemma 1 in [30], we have the conditional temporal correlation coefficient $\rho(\tau \mid w_\tau)$ as

$$\rho(\tau \mid w_\tau) = \frac{p\int_{\mathbb{R}^2} g(x)g(x+\bar{v}w_\tau)\mathrm{d}x}{\mathbb{E}[h^2]\int_{\mathbb{R}^2} g^2(x)\mathrm{d}x}. \tag{36}$$

Deconditioning on w_τ yields (33). Exploring $\mathbb{E}_{w_\tau}[g(x+\bar{v}w_\tau)]$ in (33), we obtain that ρ_τ decreases monotonically with $\bar{v}$. Hence ρ_τ is upper bounded by

$$\rho_\tau \leqslant \lim_{\bar{v}\to 0}\frac{p\int_{\mathbb{R}^2} g(x)\mathbb{E}_{w_\tau}[g(x+\bar{v}w_\tau)]\mathrm{d}x}{\mathbb{E}[h^2]\int_{\mathbb{R}^2} g^2(x)\mathrm{d}x} = \frac{p}{\mathbb{E}[h^2]}.$$

Proposition 7 is then proved. □

The spatio-temporal correlation coefficient of the interference at two given locations is provided in [30, (11)]. For mobile networks, the random position difference of the nodes in different time slots needs to be averaged

out. The difference between the static and mobile networks is that in a static network, the path loss $g(x)$ does not change in one realization, while $g(x(t))$ is time variant in a mobile network. The correlation coefficient is independent of the intensity λ_0, since the interference scales linearly with λ_0.

For a time difference τ, we express the pdf of w_τ as the sum of an atmoic and a diffuse part:

$$f_{w_\tau}(z) = \sum_{i=1}^{K} a_i \delta(z - z_i) + \tilde{f}(z), \tag{37}$$

where $\sum_i a_i \leqslant 1$ and a_i ($a_i > 0$) are the probability masses of w_τ at z_i; z_i are ordered according to the Euclidean distance to the origin ($0 \leqslant \|z_1\| \leqslant \|z_2\| \leqslant \cdots$); $\delta(\cdot)$ is an impulse function; $\tilde{f}(z)$ is right-continuous at z.

We also let $d \triangleq \mathcal{H}(\mathrm{supp}(w_\tau))$, where $\mathcal{H}(\cdot)$ is the Hausdorff dimension and $\mathrm{supp}(x)$ is the support of the random variable x. We restrict ourselves to $d \in \{0, 1, 2\}$. We now have the following theorem about the scaling property of ρ_τ.

Theorem 8. *If $K \geqslant 1$ and $z_1 = 0$, we have*

$$\rho_\tau \sim \frac{a_1 p}{\mathbb{E}[h^2]}, \qquad \bar{v} \to \infty, \tag{38}$$

where $a_1 = \mathbb{P}(w_\tau = 0)$. For $d = 2$ and $z_1 > 0$ (or $K = 0$), we have

$$\rho_\tau \bar{v}^2 \sim \frac{p f_{w_\tau}(0) \delta \epsilon^\delta \pi^2}{\mathbb{E}[h^2](1-\delta)\sin(\pi\delta)}. \tag{39}$$

If $f_{w_\tau}(0) = 0$, we have

$$\rho_\tau \in o\left(\bar{v}^{-d}\right). \tag{40}$$

If $f_{w_\tau}(0) > 0$, we have

$$\rho_\tau \in \Omega\left(\bar{v}^{-d}\right). \tag{41}$$

For $d \in \{1, 2\}$, $K = 0$, and $f_{w_\tau}(0) > 0$, we have

$$\rho_\tau \in \Theta\left(\bar{v}^{-d}\right). \tag{42}$$

Proof: Rewriting $\mathbb{E}_{w_\tau}[g(x + \bar{v} w_\tau)]$, we have

$$\begin{aligned}\mathbb{E}_{w_\tau}[g(x+\bar{v}w_\tau)] &= \sum_{i=1}^{K} a_i g(x+\bar{v}z_i) + \int_{\mathbb{R}^d} \frac{\tilde{f}(z)}{\epsilon + \|x+\bar{v}z\|^\alpha} \mathrm{d}z \\ &= \sum_{i=1}^{K} a_i g(x+\bar{v}z_i) + \frac{1}{\bar{v}^d} \int_{\mathbb{R}^d} \frac{\tilde{f}(t/\bar{v})}{\epsilon + \|x+t\|^\alpha} \mathrm{d}t\end{aligned} \tag{43}$$

Inserting this in (33) yields (38), (40), (41), and (42). For $d = 2$ and $z_1 > 0$, we have

$$\lim_{\bar{v}\to\infty} \rho \bar{v}^2 = \frac{p f_{w_\tau}(0) \left(\int_{\mathbb{R}^2} g(x)\mathrm{d}x\right)^2}{\mathbb{E}[h^2]\mathbb{R}^2 g^2(x)\mathrm{d}x},$$

which yields (39), since

$$\int_{\mathbb{R}^2} g(x)\mathrm{d}x = \frac{\delta\pi^2}{\epsilon^{1-\delta}\sin(\pi\delta)},$$

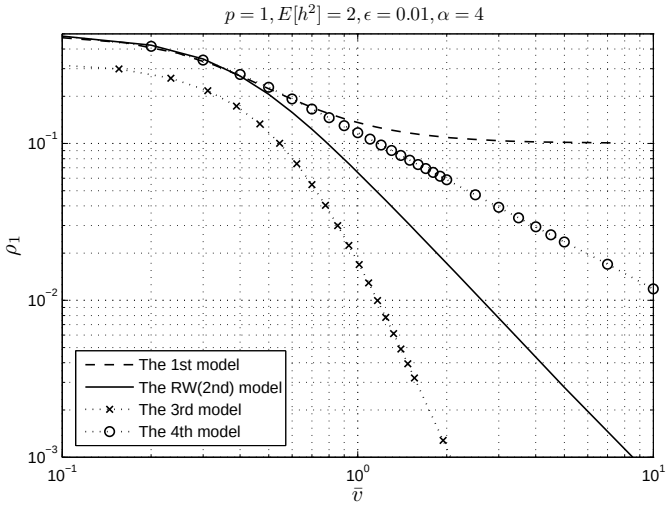

Fig. 6. The temporal correlation coefficient ρ_1 versus the mean speed $\bar{v}$ under different mobility models.

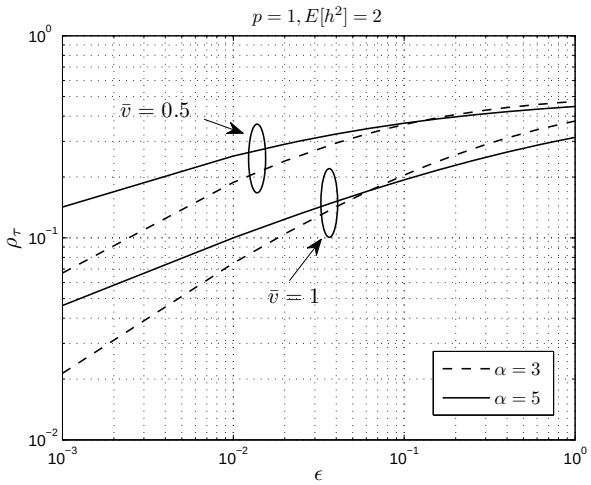

Fig. 7. The temporal correlation coefficient ρ_τ versus ϵ under the CIM model.

and

$$\int_{\mathbb{R}^2} g^2(x)\mathrm{d}x = \frac{\delta(1-\delta)\pi^2}{\epsilon^{2-\delta}\sin(\pi\delta)}.$$

Theorem 8 is then proved. □

If a node stays in the same location in time s and t with positive probability, ρ_τ converges to a constant when $\bar{v}$ goes large, since the static portion asymptotically dominates the temporal correlation. On the other hand, if a node moves to other locations with probability 1, the decay of ρ_τ depends on the Hausdorff dimension d and $f_{w_\tau}(0)$. Given $\tau = 1$, Fig. 6 shows ρ_1 versus $\bar{v}$ under different artificial mobility models, which are described in Table 5.1.

Fig. 7 shows ρ_τ versus ϵ. When ϵ is small, ρ_τ increases with α. For α not too close to 2, interferers close to the origin dominate the interference. Such dominance is more prominent with larger α and hence causes higher temporal correlation of the interference. However, ρ_τ

Models	d	$f_{w_1}(z)$	Scaling property
The 1st model	2	$0.2\delta(z)+0.8\tilde{f}(z)$, where $\tilde{f}(z)=\begin{cases}\frac{1}{\pi R_1^2} & \|z\|\leqslant R_1\\ 0 & \text{otherwise,}\end{cases}$ where $R_1=15/8$	$\rho_1 \sim \frac{0.2p}{\mathbb{E}[h^2]}$
The RW model	2	$\tilde{f}(z)=\begin{cases}\frac{1}{\pi R_{\mathrm{RW}}^2} & \|z\|\leqslant R_{\mathrm{RW}}\\ 0 & \text{otherwise}\end{cases}$	$\rho_1\bar{v}^2 \sim \frac{p\delta\epsilon^\delta\pi}{\mathbb{E}[h^2](1-\delta)R_{\mathrm{RW}}^2\sin(\pi\delta)}$
The 3rd model	2	$\tilde{f}(z)=\begin{cases}\frac{4}{3\pi R_3^2} & R_3/2\leqslant\|z\|\leqslant R_3\\ 0 & \text{otherwise,}\end{cases}$ where $R_3=9/7$	$\rho_1\in o\left(\bar{v}^{-2}\right)$
The 4th model	1	$\tilde{f}(z)=\begin{cases}\frac{1}{4} & \|z\|\leqslant 2\\ 0 & \text{otherwise}\end{cases}$	$\rho_1\in\Theta\left(\bar{v}^{-1}\right)$

TABLE 1
Four types of mobility models.

decreases with α when ϵ is large. More nodes contribute to the interference in this case. For large ϵ, the smaller the path loss exponent, the more correlated the interference is.

The integral $\int_{\mathbb{R}^2} g(x)\mathbb{E}_{w_\tau}[g(x+\bar{v}w_\tau)]\mathrm{d}x$ in (33) depends on the mobility models. In the next several subsections, we discuss different mobility models individually.

5.1.1 Constrained i.i.d. mobility (CIM)

Corollary 9. *The temporal correlation coefficient under the CIM model $\rho_{\tau,\mathrm{CIM}}$, where $\tau\geqslant 1$, is upper bounded by*

$$\rho_{\tau,\mathrm{CIM}} \lesssim \frac{p}{\mathbb{E}[h^2]}\cdot\min\left\{1,\frac{\delta\pi\epsilon^\delta}{(1-\delta)R_{\mathrm{CIM}}^2\sin(\pi\delta)\bar{v}^2}\right\}, \quad (44)$$

where $R_{\mathrm{CIM}}=45\pi/128$.

Proof: From (43) and the fact that $f_{w_\tau}(0)\geqslant f_{w_\tau}(x)$,

$$\mathbb{E}_{w_\tau}[g(x+\bar{v}w_\tau)] \leqslant \frac{1}{\bar{v}^2}\int_{\mathbb{R}^2}\frac{f_{w_\tau}(0)}{\epsilon+\|x+t\|^\alpha}\mathrm{d}t. \quad (45)$$

(44) follows from Theorem 8 after several steps of calculation, since $f_{w_\tau}(0)=1/\pi R_{\mathrm{CIM}}^2$. □

Fig. 8 shows the numerical evaluation of $\rho_{\tau,\mathrm{CIM}}$ from (33) (solid curves) together with the upper bound from (44) (dashed curves). The curves converge to the upper bound fast as $\bar{v}$ increases.

From (33) and (44), we find that the temporal correlation under the CIM model, $\rho_{\tau,\mathrm{CIM}}$, is independent of τ. This observation is in agreement with the definition of the CIM model. For the Nakagami-m fading model, we have $\mathbb{E}[h^2]=\frac{m+1}{m}$. In particular, $\mathbb{E}[h^2]=2$ for Rayleigh fading ($m=1$), and $\mathbb{E}[h^2]=1$ for no fading ($m\to\infty$). $\rho_{\tau,\mathrm{CIM}}$ increases with m, as well as with the MAC scheme parameter p. Both fading and random MAC scheduling schemes reduce the temporal correlation of the interference.

5.1.2 Random walk (RW)

Under the RW model, we focus on the temporal correlation of the interference between two successive time slots, *i.e.*, ρ_1. By a similar derivation as for the CIM model, we have the following corollary about $\rho_{1,\mathrm{RW}}$.

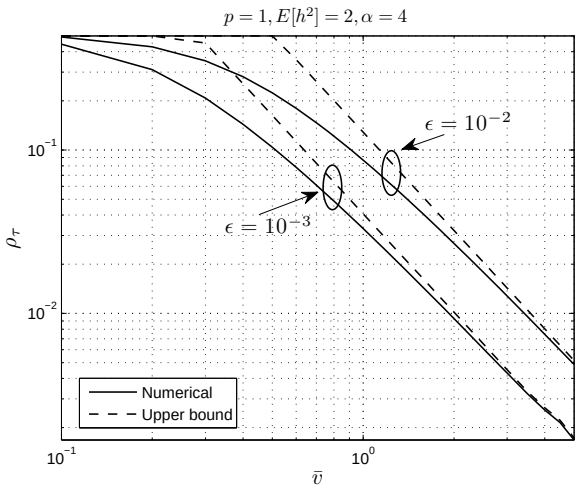

Fig. 8. Numerical evaluation (from (33)) of the temporal correlation coefficient ρ_τ versus the mean node speed $\bar{v}$ with the corresponding upper bound (from (44)). The mobility model is CIM.

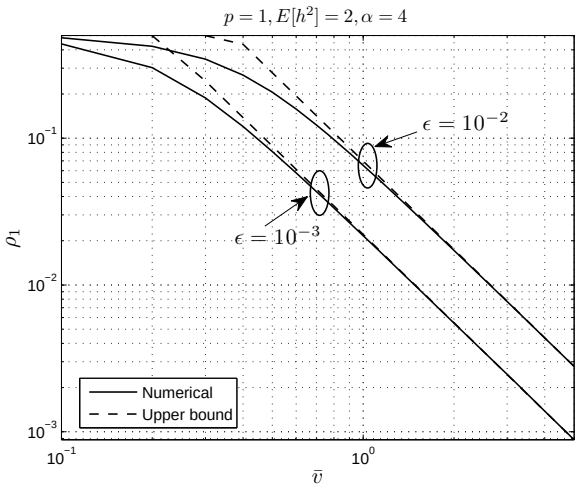

Fig. 9. Numerical evaluation (from (33)) of the temporal correlation coefficient ρ_1 versus the mean node speed $\bar{v}$ with the corresponding upper bound (from (46)). The mobility model is RW.

Corollary 10. *The temporal correlation coefficient under the RW model $\rho_{1,\mathrm{RW}}$ is upper bounded by*

$$\rho_{1,\mathrm{RW}} \lesssim \frac{p}{\mathbb{E}[h^2]} \cdot \min\left\{1, \frac{4\delta\pi\epsilon^{\delta}}{9(1-\delta)\sin(\pi\delta)\bar{v}^2}\right\}. \quad (46)$$

Proof: The calculation is straightforward following the proof of Corollary 9 since $f_{w_1}(0) = 1/\pi R_{\mathrm{RW}}^2$. □

Fig. 9 displays the numerical evaluation of $\rho_{1,\mathrm{RW}}$ from (33) and its upper bound from (46). Again the convergence is fast.

5.1.3 Discrete-time Brownian motion (BM)

Under the BM model, we have

$$w_\tau = \sum_{i=1}^{\tau} w(i) \overset{(d)}{=} \sqrt{\tau} w_0,$$

where $\overset{(d)}{=}$ denotes the equality in distribution and w_0 is a two-dimensional Gaussian random variable, *i.e.*, $\mathcal{N}(0, \sigma^2\mathbf{I})$, where $\mathbf{I}$ is the 2-by-2 identity matrix. Hence, (33) can be rewritten as

$$\rho_{\tau,\mathrm{BM}} = \frac{p\int_{\mathbb{R}^2} g(x)\,\mathbb{E}_{w_0}[g(x+\sqrt{\tau}\bar{v}w_0)]\,\mathrm{d}x}{\mathbb{E}[h^2]\int_{\mathbb{R}} g^2(x)\mathrm{d}x}. \quad (47)$$

Fig. 10 plots ρ_1 versus the mean speed of nodes $\bar{v}$ under three mobility models. As we observe from the figure, ρ_1 under these three models are asymptotically proportional to $\bar{v}^{-2}$. At an identical speed level, ρ_1 under these three models are close. For large τ, we have the following corollary about $\rho_{\tau,\mathrm{BM}}$.

Corollary 11. *When the time difference $\tau \to \infty$, the temporal correlation coefficient under the BM model is given by*

$$\rho_{\tau,\mathrm{BM}} \sim C\tau^{-1}, \quad (48)$$

where

$$C = \frac{\pi^2\epsilon^{\delta}}{\delta(1-\delta)\sin(\pi\delta)\bar{v}^2},$$

and $\rho_{\tau,\mathrm{BM}}$ is upper bounded by

$$\rho_{\tau,\mathrm{BM}} \lesssim \frac{p}{\mathbb{E}[h^2]} \cdot \min\left\{1, \frac{\pi^2\epsilon^{\delta}}{\delta(1-\delta)\sin(\pi\delta)\tau\bar{v}^2}\right\}. \quad (49)$$

Proof: Based on Theorem 8, (48) and (49) follow from (47) after a few elementary steps. □

5.2 Outage correlation

In the design of retransmission schemes in wireless networks, it is often assumed that outage events are independent across time for the sake of mathematical simplicity. However, due to the temporal correlation of the interference, link outage events are temporally correlated as well. Intuitively speaking, a link in outage at a given time indicates a higher outage probability in the next several time slots. Such correlation affects retransmission and routing schemes greatly and thus needs to be quantified. The correlation of link outage in static networks is examined in [30]. In this section, we discuss the temporal correlation of the outage in mobile networks. Rayleigh fading is assumed in the analysis.

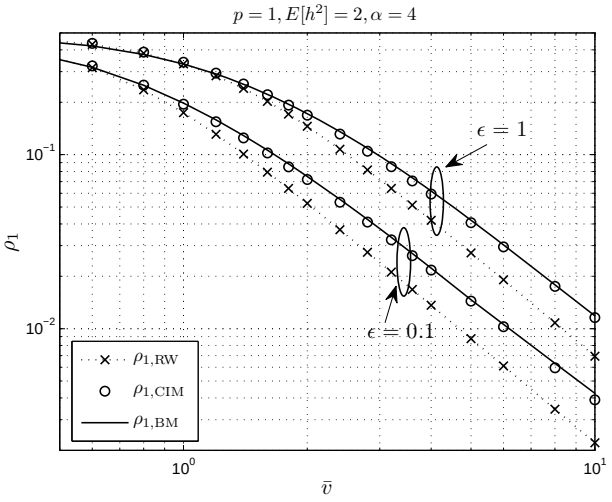

Fig. 10. The interference correlation coefficient ρ_1 versus the mean speed $\bar{v}$ under three mobility models.

Let A_t denote the event that the link is in outage at time t, *i.e.*, $A_t \triangleq \left\{\mathrm{SIR}(t) = \frac{h(t)}{I(t)} < \theta\right\}$, where the distance of the desired link is normalized to one as indicated in Section 2.1. The joint probability of the events A_s and A_t is given in (50) in the next page, where (a) follows from the independence of $h(s)$ and $h(t)$; (b) follows from the identical distribution of $I(t)$ and $I(s)$; (c) follows from the averaging over T_x and h_x; (d) holds from the probability generating functional (pgfl) of the PPP.

The direct evaluation of (50) seems hopeless, since the joint distribution of the two correlated random variables $I(t)$ and $I(s)$ is hard to obtain. However, we find that $\mathbb{P}(A_s, A_t)$ is upper bounded by the joint outage probability in static networks.

Proposition 12. *The conditional outage probability $\mathbb{P}(A_t \mid A_s)$ is upper bounded by*

$$\mathbb{P}(A_t \mid A_s) \leqslant 1 - \mathcal{L}_I(\theta) + \frac{(B-1)\mathcal{L}_I^2(\theta)}{1-\mathcal{L}_I(\theta)}, \quad (51)$$

where

$$B \triangleq \exp\left(\lambda_0 p^2 \int_{\mathbb{R}^2}\left(\frac{\theta g(x)}{1+\theta g(x)}\right)^2 \mathrm{d}x\right) = \exp\left(\frac{\delta\pi^2(1-\delta)\theta^2\lambda_0 p^2}{(\epsilon+\theta)^{2-\delta}\sin(\pi\delta)}\right). \quad (52)$$

Proof: We have

$$\mathbb{P}(A_t \mid A_s) = \frac{\mathbb{P}(A_t, A_s)}{\mathbb{P}(A_t)} \leqslant \lim_{\bar{v}\to 0}\frac{\mathbb{P}(A_t, A_s)}{\mathbb{P}(A_t)}.$$

The calculation of the joint outage probability in static networks ($\lim_{\bar{v}\to 0}\mathbb{P}(A_s, A_t)$) is similar to [30, Section IV] under the non-singular path-loss model. □

Corollary 13. *The conditional outage probability $\mathbb{P}\left(A_t \mid \bar{A}_s\right)$*

$$
\begin{aligned}
\mathbb{P}(A_s, A_t) &= \mathbb{P}(h(s) < \theta I(s), h(t) < \theta I(t)) \\
&\overset{(a)}{=} \mathbb{E}_{I(s),I(t)}\left[(1-\exp\left(-\theta I(s)\right))(1-\exp\left(-\theta I(t)\right))\right], \\
&\overset{(b)}{=} 1 - 2\mathbb{E}[\exp(-\theta I(t))] + \\
&\quad \mathbb{E}\left[\exp\left(-\theta \sum_{x\in\Phi(s)} \left(T_x(s)h_x(s)g(x) + T_x(t)h_x(t)g(x+\bar{v}w_\tau)\right)\right)\right] \\
&\overset{(c)}{=} 1 - 2\mathcal{L}_I(\theta) + \\
&\quad \mathbb{E}\left[\prod_{x\in\Phi(s)} \left(\frac{p}{1+\theta g\left(x\right)} + 1 - p\right)\left(\frac{p}{1+\theta g\left(x+\bar{v}w_\tau\right)} + 1 - p\right)\right] \\
&\overset{(d)}{=} 1 - 2\mathcal{L}_I(\theta) + \mathbb{E}_{w_\tau}\left[\exp\left(-\lambda_0 \int_{\mathbb{R}^2} 1 - \left(\frac{p}{1+\theta g\left(x\right)} + 1 - p\right)\cdot \right.\right. \\
&\quad \left.\left.\left(\frac{p}{1+\theta g\left(x+\bar{v}w_\tau\right)} + 1 - p\right)\mathrm{d}x\right)\right]. \qquad (50)
\end{aligned}
$$

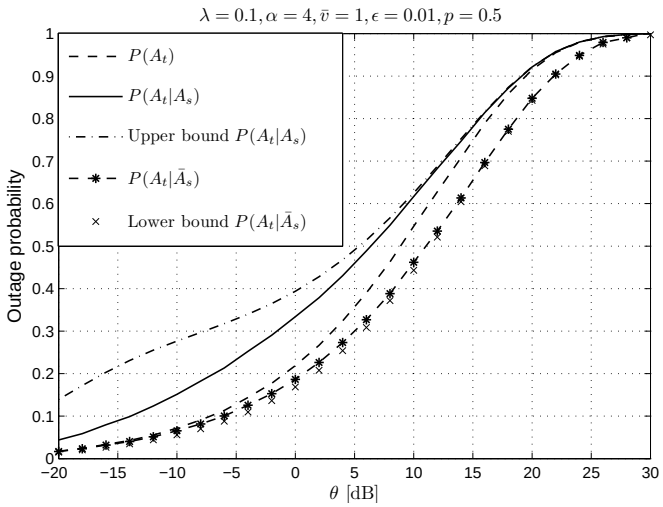

Fig. 11. The conditional outage probabilities $\mathbb{P}(A_t \mid A_s)$ and $\mathbb{P}\big(A_t \mid \bar{A}_s\big)$ together with the unconditional outage probability $\mathbb{P}(A_t)$ versus the threshold θ under the CIM model. The dashed curve is the unconditional outage probability; the dash-dotted curve is the upper bound of $\mathbb{P}(A_t \mid A_s)$ from (51); the solid-line curve is the exact expression of $\mathbb{P}(A_t \mid A_s)$ via simulations; the stars are $\mathbb{P}(A_t \mid \bar{A}_s)$ via simulations; the $\times$ is the lower bound of $\mathbb{P}\big(A_t \mid \bar{A}_s\big)$ from (53).

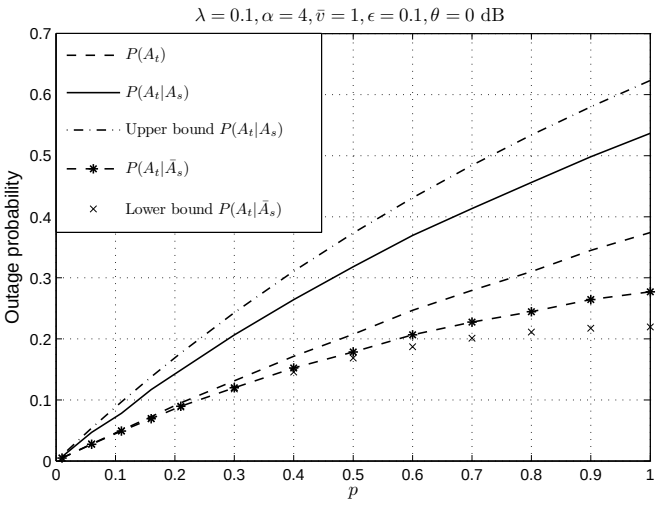

Fig. 12. The conditional outage probabilities $\mathbb{P}(A_t \mid A_s)$ and $\mathbb{P}\big(A_t \mid \bar{A}_s\big)$ together with the unconditional outage probability $\mathbb{P}(A_t)$ versus the MAC scheme parameter p under the CIM model.

is lower bounded by

$$\mathbb{P}\big(A_t \mid \bar{A}_s\big) \geqslant 1 - B\mathcal{L}_I(\theta), \qquad (53)$$

where B is from (52).

Proof: The proof is similar to the proof of Proposition 12. □

Fig. 11 and 12 display the simulation evaluations of the conditional outage probability versus the threshold θ and the MAC scheme parameter p, respectively, together with the upper and lower bounds from (51) and (53). The CIM model is used in the simulation. The unconditional outage probability $\mathbb{P}(A_t)$ is always smaller than $\mathbb{P}(A_t \mid A_s)$. The outage evaluation in a single time slot ignores the information about previous link states and thus provides an over-optimistic evaluation of the network performance. On the other hand, $\mathbb{P}(A_t) > \mathbb{P}\big(A_t \mid \bar{A}_s\big)$, as expected. The discrepancy between $\mathbb{P}(A_t \mid A_s)$ and $\mathbb{P}(A_t)$ is larger when $\mathbb{P}(A_t)$ is low (or θ is low), since the conditioning makes a larger difference in this regime. Conversely, the discrepancy between $\mathbb{P}\big(A_t \mid \bar{A}_s\big)$ and $\mathbb{P}(A_t)$ is larger when $\mathbb{P}(A_t)$ is high (θ is high). In the two extreme cases where the threshold $\theta \to \infty$ or $\theta \to 0$, the conditioning does not make a difference any more.

6 Remarks and Conclusions

In this section, we summarize the results we have obtained in this paper and draw conclusions.

- *Macroscopic mobility:* We treat macroscopic mobility from a large-scale fading perspective. Fluctuations of the path loss induced by mobility constitute another type of fading in wireless channels besides multi-path effects. To make the difference clear, we may speak of fading induced by microscopic mobility (multi-path fading) and fading induced by macroscopic mobility.
- *Mean interference and outage probability:* The mean interference at the origin under the RWP model is asymptotically twice the interference under UMM, which leads to higher outage probability, while the interference at the border is lower. Also for RWP, the interference at the border decreases to zero as the network radius goes large. These observations lead us to an important research direction: the design of location-aware routing algorithms. However, the decreasing interference is due to the smaller node intensity near the border, which means that fewer nodes can be chosen as receivers. The trade-off between the locations of destinations (or relays) and the interference should be considered.
- *Temporal correlation of interference:* The mobility models affect the correlation coefficient of the interference ρ. The more degrees of freedom the node explores, the faster ρ decays with the mobility range. Multi-path fading and random MAC schemes also reduce the interference correlation.
- *Temporal correlation of outage:* Conditioned on the link being in outage at time t, the outage probability in the next several time slots is higher compared to the unconditional outage probability. On the other hand, if a transmission is successful, the conditional success probability is higher in the next several time slots. Hence, the design of new retransmission schemes with correlation-awareness is important. For example, if a transmission is successful, the node should transmit more often in successive time slots (higher transmit probability) in order to take advantage of the outage (success) correlation. Conversely, if a link is in outage, several silence slots should be added before the transmitter starts another try, since blind retransmission worsens the network performance. If fewer transmitters are concurrent, the success probability increases due to the decreased interference power. It in turn lowers the number of retransmissions. The trade-off between delay and network throughput, and fairness and throughput should be explored as well.

ACKNOWLEDGMENTS

The support of the NSF (grants CNS 1016742 and CCF 1216407) is gratefully acknowledged.

References

[1] D. Tse and P. Viswanath, *Fundamentals of wireless communication*. Cambridge University Press, 2005.

[2] M. Haenggi, J. G. Andrews, F. Baccelli, O. Dousse, and M. Franceschetti, "Stochastic Geometry and Random Graphs for the Analysis and Design of Wireless Networks," *IEEE Journal on Selected Areas in Communications*, vol. 27, pp. 1029-1046, Sept. 2009.

[3] F. Baccelli, and B. Blaszczyszyn, *Stochastic Geometry and Wireless Networks Volume II: Applications*. Foundations and Trends in Networking (NOW Publishers), vol. 4, no. 1-2, pp. 1-312, 2009.

[4] M. Chiang, P. Hande, T. Lan, and C. W. Tan, *Power control in wireless cellular networks*. Foundations and Trends in Networking (NOW Publishers), vol.2, no. 4, pp. 381-533, 2008.

[5] M. Haenggi and R. K. Ganti, *Interference in Large Wireless Networks*. Foundations and Trends in Networking (NOW Publishers), vol. 3, no. 2, pp. 127-248, 2009.

[6] X. Zhang and M. Haenggi, "Random Power Control in Poisson Networks," *IEEE Transactions on Communications*, vol. 60, pp. 2602-2611, Sept. 2012.

[7] R. M. Metcalfe and D. R. Boggs, "Ethernet: Distributed packet switching for local computer networks,", *Communications of the ACM*, vol. 19, no. 7, pp. 395-404, 1976.

[8] L. Kleinrock and F. Tobagi, "Packet switching in radio channels: Part I–carrier sense multiple-access modes and their throughput-delay characteristics," *IEEE Transactions on Communications*, vol. 23, no. 12, pp. 1400-1416, 1975.

[9] M. Haenggi, *Stochastic Geometry for Wireless Networks*. Cambridge University Press, 2012.

[10] M. Penrose, *Random geometric graphs*. Oxford University Press, USA, 2003.

[11] E. Sousa and J. Silvester, "Optimum transmission ranges in a direct sequence spread-spectrum multihop packet radio network," *IEEE Journal on Selected Areas in Communications*, vol. 8, pp.762-771, Jun. 1990.

[12] E. Sousa, "Interference modeling in a direct-sequence spread-spectrum packet radio network," *IEEE Transactions on Communications*, vol. 38, no.9 pp. 1475-1482, 1992.

[13] F. Baccelli, B. Blaszczyszyn, and P. Muhlethaler, "An Aloha protocol for multihop mobile wireless networks," *IEEE Transactions on Information Theory*, vol. 52, no. 2, pp. 421-436, 2006.

[14] M. Zorzi and S. Pupolin, "Optimum transmission ranges in multihop packet radio networks in the presence of fading," *IEEE Transactions on Communications*, vol. 43, no. 7, pp. 2201-2205, 2002.

[15] S. Srinivasa and M. Haenggi, "Distance Distributions in Finite Uniformly Random Networks: Theory and Applications," *IEEE Transactions on Vehicular Technology*, vol. 59, pp. 940-949, Feb. 2010.

[16] R. K. Ganti and M. Haenggi, "Interference and Outage in Clustered Wireless Ad Hoc Networks," *IEEE Transactions on Information Theory*, vol. 55, pp. 4067-4086, Sept. 2009.

[17] R. K. Ganti and M. Haenggi, "Interference in Ad Hoc Networks with General Motion-Invariant Node Distributions," in *2008 IEEE International Symposium on Information Theory (ISIT'08)*, (Toronto, Canada), July 2008.

[18] R. Giacomelli, R. K. Ganti, and M. Haenggi, "Outage Probability of General Ad Hoc Networks in the High-Reliability Regime," *IEEE/ACM Transactions on Networking*, vol. 19, pp. 1151-1163, Aug. 2011.

[19] R. K. Ganti, J. G. Andrews, and M. Haenggi, "High-SIR Transmission Capacity of Wireless Networks with General Fading and Node Distribution," *IEEE Transactions on Information Theory*, vol. 57, pp. 3100-3116, May 2011.

[20] C.-H. Lee and M. Haenggi, "Interference and Outage in Poisson Cognitive Networks," *IEEE Transactions on Wireless Communications*, vol. 11, pp. 1392-1401, Apr. 2012.

[21] H. Nguyen, F. Baccelli, and D. Kofman, "A stochastic geometry analysis of dense IEEE 802.11 networks," in *IEEE INFOCOM*, pp. 1199-1207, 2007.

[22] O. Dousse, M. Franceschetti, and P. Thiran, "On the throughput scaling of wireless relay networks," *IEEE/ACM Transactions on Networking*, vol. 14, no. 6, pp. 2756-2761, 2006.

[23] R. K. Ganti and M. Haenggi, "Spatial Analysis of Opportunistic Downlink Relaying in a Two-Hop Cellular System," *IEEE Transactions on Communications*, vol. 60, pp. 1443-1450, May 2012.

[24] F. Baccelli and C. Bordenave, "The radial spanning tree of a Poisson point process," *Annals of Applied Probability*, vol. 17, no. 1, pp. 305-369, 2007.
[25] M. Haenggi, "On Routing in Random Rayleigh Fading Networks," *IEEE Transactions on Wireless Communications*, vol. 4, pp. 1553-1562, July 2005.
[26] F. Baccelli, B. Blaszczyszyn, and P. Muhlethaler, "On the performance of time-space opportunistic routing in multihop mobile ad hoc networks," in *7th International Symposium on Modeling and Optimization in Mobile, Ad Hoc, and Wireless Networks (WiOpt'09)*, Berlin, 2008.
[27] S. P. Weber, X. Yang, J. G. Andrews and G. De Veciana, "Transmission capacity of wireless ad hoc networks with outage constraints," *IEEE Transactions on Information Theory*, vol. 51, no. 12, ppp. 4019-4102, 2005.
[28] M. Haenggi, "Outage, Local Throughput, and Capacity of Random Wireless Networks," *IEEE Transactions on Wireless Communications*, vol. 8, pp. 4350-4359, Aug. 2009.
[29] R. K. Ganti and M. Haenggi, "Limit of the Transport Capacity of a Dense Wireless Network," *Journal of Applied Probability*, vol. 47, pp. 886-892, Sept. 2010.
[30] R. K. Ganti and M. Haenggi, "Spatial and temporal correlation of the interference in ALOHA ad hoc networks," *IEEE Communications Letters*, vol. 13, no. 9, pp. 631-633, 2009.
[31] R. K. Ganti, and J. G. Andrews, "Correlation of link outage in low-mobility spatial wireless networks," in *Asilomar Conference on Signals, Systems, and Computers*, (Pacific Grove), Nov. 2010.
[32] U. Schilcher, and G. Brandner, and C. Bettstetter, "Temporal correlation of the interference in wireless networks with Rayleigh block fading," *IEEE Transactions on Mobile Computing*, vol. 11, pp. 2109-2120, Dec. 2012.
[33] M. Haenggi, "Diversity loss due to interference correlation," *IEEE Communications Letters*, vol. 16, pp. 1600-1603, Oct. 2012.
[34] Z. Kong and E. M. Yeh, "On the latency for information dissemination in mobile wireless networks," in *Proceedings of the 9th ACM International Symposium on Mobile Ad Hoc Networking and Computing (MobiHoc)*, Hong Kong SAR, China, May 2008.
[35] T. Camp, J. Boleng, and V. Davies, "A survey of mobility models for ad hoc network research Research," *Wireless Communications and Mobile Computing*, vol. 2, no. 5, pp. 483-502, 2002.
[36] S. Bandyopadhyay, E. J. Coyle, and T. Falck, "Stochastic properties of mobility models in mobile ad hoc networks," *IEEE Transactions on Mobile Computing*, vol. 6, no. 11, pp. 1218-1229, 2007.
[37] C. Bettstetter, "Mobility modeling in wireless networks: categorization, smooth movement, and border effects," *ACM SIGMOBILE Mobile Computing and Communications Review*, vol. 5, no. 3, p. 66, 2001.
[38] C. Bettstetter, G. Resta, and P. Santi, "The node distribution of the random waypoint mobility model for wireless ad hoc networks," *IEEE Transactions on Mobile Computing*, vol. 2, no. 3, pp. 257-269, 2003.
[39] C. Bettstetter, "On the connectivity of ad hoc networks," *The Computer Journal*, vol. 47, no. 4, p. 432, 2004.
[40] E. Hyytia and P. Lassila and J. Virtamo, "Spatial node distribution of the random waypoint mobility model with applications," *IEEE Transactions on Mobile Computing*, vol. 5, no. 6, pp. 680-694, 2006.
[41] M. Haenggi, "A Geometric Interpretation of Fading in Wireless Networks: Theory and Applications," *IEEE Transactions on Information Theory*, vol. 54, pp. 5500-5510, Dec. 2008.
[42] P. Nain, D. Towsley, B. Liu, Z. Liu, and F. Inria, "Properties of random direction models," *IEEE INFOCOM*, vol. 3, 2005.

Zhenhua Gong (S'10) received the B.S. degree in electrical engineering from Shanghai Jiao Tong University, Shanghai, China, in 2007. Since 2007, he has been with the Department of Electrical Engineering, University of Notre Dame, Notre Dame, IN, where he is working towards the Ph.D. degree. His research interests include the analysis and design of cellular and sensor networks. Specifically, he focuses on the stochastic geometry for the performance analysis of mobile networks under interference constraints. Besides the theoretical research, he is also involved in the implementation of multi-user techniques in wireless networks.

Martin Haenggi (S'95, M'99, SM'04) is a Professor of Electrical Engineering and a Concurrent Professor of Applied and Computational Mathematics and Statistics at the University of Notre Dame, Indiana, USA. He received the Dipl.-Ing. (M.Sc.) and Dr.sc.techn. (Ph.D.) degrees in electrical engineering from the Swiss Federal Institute of Technology in Zurich (ETH) in 1995 and 1999, respectively. After a postdoctoral year at the University of California in Berkeley, he joined the University of Notre Dame in 2001. In 2007-2008, he spent a Sabbatical Year at the University of California at San Diego (UCSD). For both his M.Sc. and his Ph.D. theses, he was awarded the ETH medal, and he received a CAREER award from the U.S. National Science Foundation in 2005 and the 2010 IEEE Communications Society Best Tutorial Paper award.

He served as a member of the Editorial Board of the Elsevier Journal of Ad Hoc Networks from 2005-2008 and as an Associate Editor for the IEEE Transactions on Mobile Computing (TMC) from 2008-2011 and for the ACM Transactions on Sensor Networks from 2009-2011 and as a Guest Editor for the IEEE Journal on Selected Areas in Communications in 2008-2009 and the IEEE Transactions on Vehicular Technology in 2012-2013. He also served as a Distinguished Lecturer for the IEEE Circuits and Systems Society in 2005-2006, as a TPC Co-chair of the Communication Theory Symposium of the 2012 IEEE International Conference on Communications (ICC'12), and as a General Co-chair of the 2009 International Workshop on Spatial Stochastic Models for Wireless Networks and the 2012 DIMACS Workshop on Connectivity and Resilience of Large-Scale Networks. Presently he is a Steering Committee Member of TMC. He is a co-author of the monograph "Interference in Large Wireless Networks" (NOW Publishers, 2009) and the author of the textbook "Stochastic Geometry for Wireless Networks" (Cambridge University Press, 2012). His scientific interests include networking and wireless communications, with an emphasis on ad hoc, cognitive, cellular, sensor, and mesh networks.